


## Article

# Influence of Solvent-Dependent Morphology on Molecular Doping and Charge Transport in Conductive Thiophene Polymer

Haoyu Chai <sup>1,2</sup>, Hui Li <sup>2,\*</sup> , Fei Zhong <sup>2</sup>, Zhen Xu <sup>2</sup>, Shengqiang Bai <sup>2,3</sup> and Lidong Chen <sup>2,3</sup>

<sup>1</sup> School of Materials Science and Engineering, Jingdezhen Ceramic University, Jingdezhen 333403, China; 1920024009@stu.jci.edu.cn

<sup>2</sup> State Key Laboratory of High Performance Ceramics and Superfine Microstructure, Shanghai Institute of Ceramics, Chinese Academy of Sciences, Shanghai 200050, China; zhongfei21@mails.ucas.ac.cn (F.Z.); xuzhen20@mails.ucas.ac.cn (Z.X.); bsq@mail.sic.ac.cn (S.B.); cld@mail.sic.ac.cn (L.C.)

<sup>3</sup> Center of Materials Science and Optoelectronics Engineering, University of Chinese Academy of Sciences, Beijing 100049, China

\* Correspondence: lihui889@mail.sic.ac.cn

**Abstract:** The utility of a solvent is one of the key factors that impacts resultant film morphology. However, the effect of solvent-dependent morphology on the doping process and electrical conductivity has not been adequately elucidated. In this work, we compared the morphology of chloroform- and chlorobenzene-processed thiophene polymer films and investigated how the choice of solvent influences film morphology, doping level, charge transport properties, and thus electrical conductivity. It was found that the film drop-casted from chloroform exhibits better crystallinity than that drop-casted from chlorobenzene. The crystallinity has negligible impact on the doping level but significant impact on charge transport properties. As a result, the chloroform-processed film shows a higher electrical conductivity of up to  $408 \text{ S cm}^{-1}$  due to a high carrier mobility related to the continuously crystalline domains in film. This finding indicates that the choice of solvent for preparation of film, which strongly correlated with molecular orientation, is a new strategy to optimize the electrical conductivity of doped polymers.

**Keywords:** conductive polymer; chemical doping; electrical conductivity; carrier mobility



**Citation:** Chai, H.; Li, H.; Zhong, F.; Xu, Z.; Bai, S.; Chen, L. Influence of Solvent-Dependent Morphology on Molecular Doping and Charge Transport in Conductive Thiophene Polymer. *Materials* **2022**, *15*, 3293. <https://doi.org/10.3390/ma15093293>

Academic Editor: Swarup Roy

Received: 8 April 2022

Accepted: 1 May 2022

Published: 4 May 2022

**Publisher's Note:** MDPI stays neutral with regard to jurisdictional claims in published maps and institutional affiliations.



**Copyright:** © 2022 by the authors. Licensee MDPI, Basel, Switzerland. This article is an open access article distributed under the terms and conditions of the Creative Commons Attribution (CC BY) license (<https://creativecommons.org/licenses/by/4.0/>).

## 1. Introduction

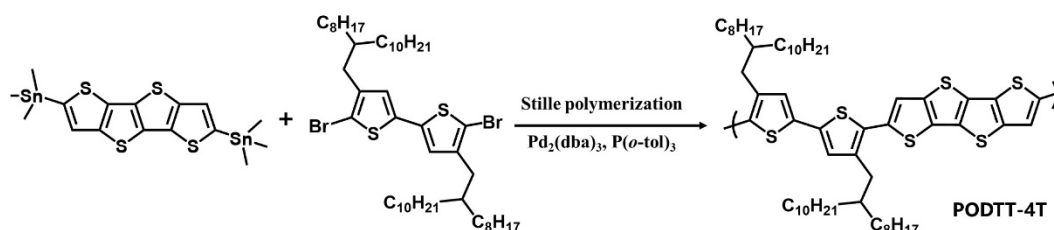
Molecular doping has been a promising way to control the electrical properties of polymer semiconductors [1,2]. The doped conjugated polymers are widely used as the active layers in the organic field-effect transistor, organic light-emitting diode, and organic thermoelectric devices [3–7]. Molecular doping will improve the electrical conductivity ( $\sigma$ ) by increasing free carriers along polymer chains via charge transfer between polymer and dopant. To achieve a high  $\sigma$ , an extremely high doping concentration is usually required to obtain a high carrier concentration ( $n$ ) [8,9]. However, the addition of large amounts of dopants results in a disruption of the polymer film morphology and induces a drop in carrier mobility ( $\mu$ ) [10], which leads to a low  $\sigma$  according to the relationship of  $\sigma = ne\mu$ . [8] Therefore, it is still challenging to effectively dope polymers without restraining the charge transport in polymer film. There have been great efforts recently to overcome film quality issues of heavily doped conjugated polymers. For example, several doping methods are developed in which the dopants are applied to a pre-casted polymer film, including vapor-phase deposition [11,12], immersion doping [13,14], sequential doping [15,16], etc. Other attention has been given to the modification of chemical structures of polymers to leave dopants in side chains without disturbing the packing of polymer backbones [17,18]. For instance, the introduction of  $\pi$ -conjugated subunits as a spacer can reduce the number of side chains and improve the accommodation of dopants into

films [19]. Additionally, polythiophenes with oligo(ethylene oxide) side chains show high electrical conductivity of up to  $100 \text{ S cm}^{-1}$  and is attributed to the good miscibility between polar side chains and dopants [20,21]. It is accepted that the crystalline film of pristine polymers is beneficial for achieving good charge transport properties. The crystalline behavior of polymers is strongly related to the properties of the solvent for dissolving the given polymer [22,23]. However, how the solvent affects the solid-state orientation of pristine film, and therefore the molecular doping and charge transport in doped film, has not been sufficiently elucidated.

Herein, we investigate the influence of solvent for dissolving the polymer on the crystallinity of pristine polymer films, doping efficiency and charge transport by employing a thiophene polymer, PODTT-4T, drop-casted from chloroform (CF) and chlorobenzene (CB) solution, respectively. It is found that the pristine film prepared from CF solution (PODTT-4T<sub>CF</sub>) shows a preferentially edge-on orientation and a highly ordered microstructure while the film prepared from CB solution (PODTT-4T<sub>CB</sub>) exhibits a lower crystallinity with both edge-on and face-on orientations inside. PODTT-4T<sub>CF</sub> film shows a much higher  $\sigma$  of up to  $408 \text{ S cm}^{-1}$  compared to that of the PODTT-4T<sub>CB</sub> ( $280 \text{ S cm}^{-1}$ ) although these two films have a similar doping level if doped by  $\text{FeCl}_3$ . The higher  $\sigma$  of doped PODTT-4T<sub>CF</sub> can be ascribed to the higher carrier mobility due to larger crystalline domains upon doping compared to the PODTT-4T<sub>CB</sub> film. We propose that the choice of solvent to dissolve PODTT-4T determines the polymer crystalline behavior in the solid state, which prefers to dominate the transport property of free carriers rather than the doping efficiency.

## 2. Synthesis and Characterization of Polymer

Polymer PODTT-4T was synthesized by Stille coupling reaction [24], copolymerizing 5,5'-dibromo-4,4'-bis(2-octyldodecyl)-2,2'-bithiophene and 2,6-bis(trimethylstannyl)thieno[2',3':4,5]thieno[3,2-*b*]thieno[2,3-*d*]thiophene (4T) (Scheme 1). The large conjugated unit is used to allow good planarity, promoting the charge delocalization. The long and branched alkyl chains ensure the solubility of copolymers in common organic solvents, such as CF and CB. The synthesis details and basic properties of the polymer are given in the supporting information. PODTT-4T shows a high number-average molecular weight ( $M_n$ ) of 22.2 kDa with a polydispersity index (PDI) of 2.08 (Figure S1). It exhibits excellent thermal stability with a decomposition temperature (5% weight loss) of about  $395 \text{ }^\circ\text{C}$  measured by thermogravimetric analysis (TGA) (Figure S2). Differential scanning calorimetry (DSC) analysis shows a melting transition peak at  $296 \text{ }^\circ\text{C}$  and a crystallization peak at  $271 \text{ }^\circ\text{C}$  during the heating and cooling cycle (Figure S3), respectively, which suggests the existence of crystalline phases in the polymer [25]. PODTT-4T shows the highest occupied molecular orbit (HOMO) level around  $-5.26 \text{ eV}$  by employing the cyclic voltammetry (CV) (Figure S4), which is beneficial for p-doping by  $\text{FeCl}_3$  [26]. The pristine films were prepared by dissolving the polymer into CF or CB with a concentration of  $5 \text{ mg mL}^{-1}$ . The polymer solution was drop-casted on the glass substrate and dried at ambient temperature. Then, the films were annealed at  $160 \text{ }^\circ\text{C}$  for 30 min in the glovebox. The doped films were prepared by immersing the annealed films into  $\text{FeCl}_3$  solution (in acetonitrile,  $5 \text{ mg mL}^{-1}$ ) for 10 min.



**Scheme 1.** The synthetic route to the polymer PODTT-4T.

### 3. Results

#### 3.1. The Doping Level of Films Prepared from Two Solvents

The doping behavior of PODTT-4T<sub>CF</sub> and PODTT-4T<sub>CB</sub> films is characterized by using UV-vis-NIR absorption spectra. It is observed that pristine PODTT-4T<sub>CF</sub> and PODTT-4T<sub>CB</sub> films show a similar absorption spectrum (Figure 1a). The maximum peak appears at 605 nm and no obvious absorption is observed over 700 nm. In addition, there is no obvious peak shift or absorption intensity change between these two films although the different solvents usually induce the wavelength shift of shoulder peaks due to the change of backbone interactions [27]. This indicates PODTT-4T chains dissolved in CF and CB probably adopt a similar  $\pi$ - $\pi$  stacking distance in the solid state. Upon doping with FeCl<sub>3</sub>, the intensity of the neutral absorption peak of PODTT-4T<sub>CF</sub> and PODTT-4T<sub>CB</sub> films is significantly bleached. Meanwhile, the absorption band ascribed to the (bi)polarons appears above 800 nm in the near-infrared region. In order to compare the doping levels of the two films, two absorption bands—neutral absorption band<sub>I</sub> (380–710 nm) and (bi)polaron absorption band<sub>II</sub> (710–2000 nm)—are assigned. The ratio (*R*) of the integral area of these two absorption bands (band<sub>II</sub>/band<sub>I</sub>) is calculated (Table S1). It is found that the doped PODTT-4T<sub>CF</sub> film and PODTT-4T<sub>CB</sub> film have a similar *R* value suggesting similar doping levels in the two films [21]. This indicates that CF and CB have a negligible effect on the polymer doping level under the same conditions. Raman spectroscopy (Figure 1b) is further employed to characterize and analyze the vibrational mode of PODTT-4T<sub>CF</sub> and PODTT-4T<sub>CB</sub> upon doping. All intensities are normalized at the vibrational peak of mode A, which corresponds to the C=C symmetric stretching vibration on the 4T core. Mode B and mode C correspond to the C=C stretching vibration and the C=C/C-C stretching/shrinking on the thiophene ring, respectively [28]. These vibrational modes are sensitive to the structural order and  $\pi$ -electron delocalization [29]. The positions of mode B and mode C of the pristine PODTT-4T<sub>CF</sub> film and PODTT-4T<sub>CB</sub> film are almost the same while mode A of PODTT-4T<sub>CB</sub> is wider than that of PODTT-4T<sub>CF</sub>, indicating more disordered structures existing in the former film. Upon doping with FeCl<sub>3</sub>, both mode A and mode C shift to much lower wavenumbers, suggesting that the benzenoid structures along the conjugated backbone are transformed into quinoid structures. It should be noted that the shift of mode C of PODTT-4T<sub>CF</sub> is more significant (Table S2) and mode A is much wider compared to those of PODTT-4T<sub>CB</sub> film, which means the dopants have a significant influence on the molecular packing of polymer chains in PODTT-4T<sub>CF</sub> film. These results demonstrate that the doping level is not dependent on the molecular orientation in PODTT-4T film.

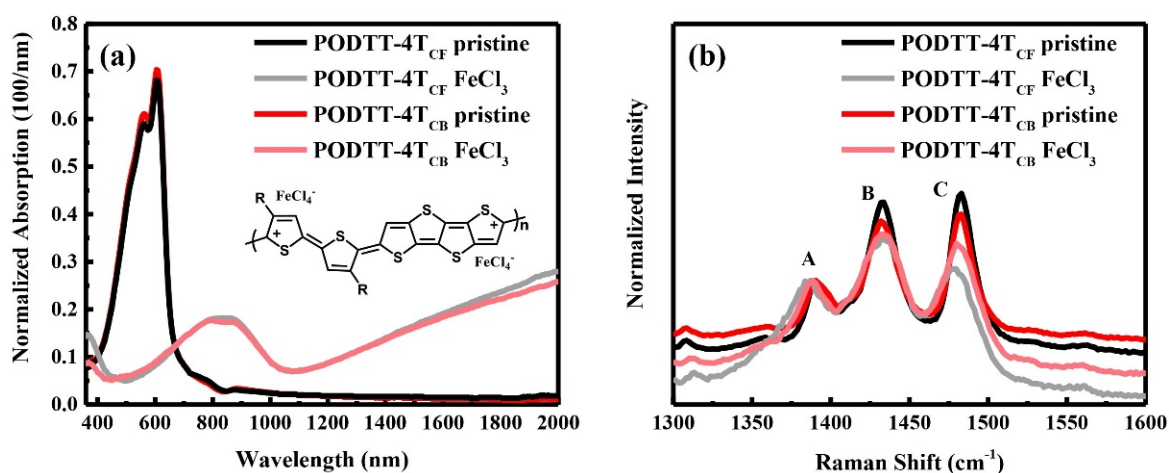


**Figure 1.** (a) The thickness-normalized absorption spectra; (b) Raman spectra of pristine and doped films drop casted from CF and CB, respectively. The Raman intensity is normalized on the band peaked at mode A.

### 3.2. The Electrical Conductivity of Doped Films

To investigate how the solvents impact the electrical properties, the electrical conductivity of PODTT-4T<sub>CF</sub> and PODTT-4T<sub>CB</sub> films doped by FeCl<sub>3</sub> was tested by four-probe measurement. As shown in Figure 2, the electrical conductivities of the two films dramatically increase with increasing the immersing time in the range of 10 min. As a result, the  $\sigma$  tend to be saturated. The  $\sigma$  of doped PODTT-4T<sub>CF</sub> film is higher than that of doped PODTT-4T<sub>CB</sub> film if doping time is greater than 10 min. The highest  $\sigma$  of PODTT-4T<sub>CF</sub> is up to 408 S cm<sup>-1</sup>, which is 1.5 times higher than that of PODTT-4T<sub>CB</sub> (280 S cm<sup>-1</sup>). In addition, the Seebeck coefficient ( $S$ , the potential difference arises from per unit temperature difference) of the doped PODTT-4T<sub>CF</sub> film is slightly higher than that of the PODTT-4T<sub>CB</sub> film (Figure S5a). As a result, the power factor ( $S^2\sigma$ ) of the doped PODTT-4T<sub>CF</sub> film is two times higher than that of the PODTT-4T<sub>CB</sub> film at a doping time of 10 min, indicating the potential thermoelectric application of this polymer. Considering a similar doping level observed in two-doped films, the higher TE performance could probably be attributed to the higher mobility in PODTT-4T<sub>CF</sub> film. To further support our hypothesis, Hall effect measurements were employed to investigate the effect of solvents on carrier concentrations and mobilities in doped polymers at doping times of 10 min (Figure S6). The results show that the mobility of the doped PODTT-4T<sub>CF</sub> film and PODTT-4T<sub>CB</sub> film is 0.96 cm<sup>2</sup> V<sup>-1</sup> s<sup>-1</sup> and 0.76 cm<sup>2</sup> V<sup>-1</sup> s<sup>-1</sup>, respectively. Meanwhile, the carrier concentration of the doped PODTT-4T<sub>CF</sub> film and PODTT-4T<sub>CB</sub> film is  $2.74 \times 10^{21}$  cm<sup>-3</sup> and  $2.62 \times 10^{21}$  cm<sup>-3</sup>, respectively (Table S3). These data indicate that both films show higher mobilities than that of a typical thiophene polymer, such as FeCl<sub>3</sub>-doped P3HT [13], due to a large and delocalized backbone of PODTT-4T. In addition, the PODTT-4T<sub>CF</sub> film exhibits a 1.3-fold higher carrier mobility with slightly more free carriers compared to PODTT-4T<sub>CB</sub> film, affirming the importance of solvent selection for electrical conductivity optimization.

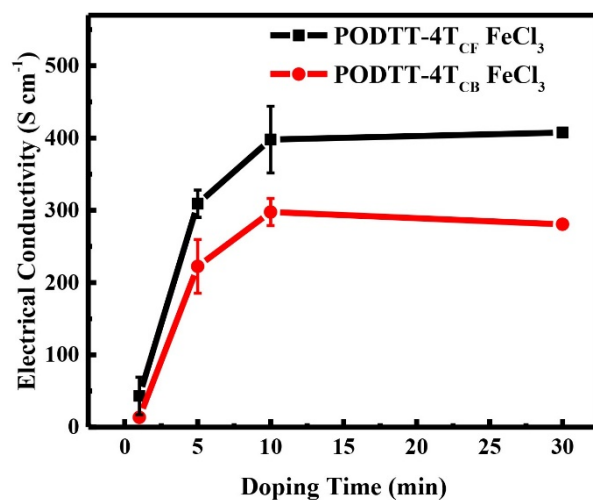


**Figure 2.** Electrical conductivities of PODTT-4T<sub>CF</sub> (black line) and PODTT-4T<sub>CB</sub> (red line) doped by FeCl<sub>3</sub> as a function of the doping time.

### 3.3. Microstructural Characterization

To further understand the relationship between solvent-dependent morphology and charge transport properties, grazing-incidence wide-angle X-ray scattering (GIWAXS) was performed (Figures 3 and S7). Pristine PODTT-4T<sub>CF</sub> film shows intense ( $h00$ ) multi-order diffraction peaks in the out-of-plane direction (along the  $q_z$  direction) and a (010) diffraction peak at  $q_{xy} = 1.6\text{--}1.8 \text{ \AA}^{-1}$  generated by  $\pi$ - $\pi$  stacking in the in-plane direction. That indicates a dominantly edge-on orientation existing in PODTT-4T<sub>CF</sub> film [30,31]. In contrast, pristine PODTT-4T<sub>CB</sub> film shows weak and broad Debye rings of ( $h00$ ) peaks with a (010) diffraction peak appearing both in the out-of-plane and in-plane directions, meaning that both edge-on and face-on orientation exists in the PODTT-4T<sub>CB</sub> film. Since CF and CB have different

boiling points, the difference of molecular orientations from two solvents can be attributed to the evaporation rate of solvent during the film preparation. In addition, the face-on orientation is thermodynamically stable packing for the polymer. The lamellar distance and  $\pi$ - $\pi$  stacking distance of the PODTT-4T<sub>CF</sub> film are 20.26 Å and 3.67 Å, while the distances are 20.93 Å and 3.67 Å for PODTT-4T<sub>CB</sub> film, respectively. (Table S4). These results demonstrate that the utility of solvent mainly affects the packing orientation in pristine films and has a negligible effect on the lamellar distance and  $\pi$ - $\pi$  stacking distance. Upon doping by FeCl<sub>3</sub>, the lamellar stacking distance of PODTT-4T<sub>CF</sub> film is increased to 22.43 Å ( $\Delta d_{100} = 2.17$  Å), while the  $\pi$ - $\pi$  stacking distance decreases to 3.50 Å ( $\Delta d_{010} = -0.17$  Å). For the PODTT-4T<sub>CB</sub> film, the lamellar packing distance is increased to 23.26 Å ( $\Delta d_{100} = 2.33$  Å) while the  $\pi$ - $\pi$  stacking distance also decreases from 3.67 to 3.50 Å ( $\Delta d_{010} = -0.17$  Å). These results indicate that the dopants prefer to intercalate into the lamellar alkyl side-chain region without disturbing the intense  $\pi$ - $\pi$  stacking attributed to the electronic coupling between the conjugated backbone. Moreover, the molecular orientations of pristine films are still maintained upon doping. The size of the crystalline grain of pristine and doped films is compared by extracting the data of the full-width at half-maximum (FWHM) of (100) peaks according to the Scherrer equation [32,33]. It is observed that the FWHM of pristine PODTT-4T<sub>CF</sub> film (0.072 Å<sup>-1</sup>) is slightly smaller than that of pristine PODTT-4T<sub>CB</sub> film (0.078 Å<sup>-1</sup>), indicating larger crystalline domains in the pristine PODTT-4T<sub>CF</sub> film. Upon doping, the crystalline domains of doped films are significantly increased. In addition, the crystalline size of doped PODTT-4T<sub>CF</sub> film is still much larger than that of doped PODTT-4T<sub>CB</sub> film.

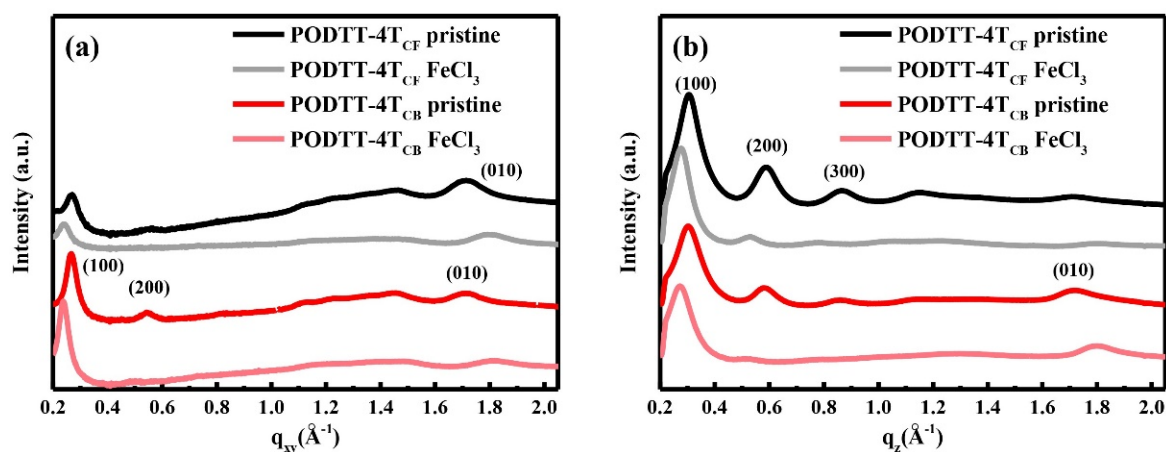


**Figure 3.** (a) GIWAXS line cuts of in-plane scattering profiles; (b) GIWAXS line cuts of out-of-plane scattering profiles of pristine and doped films drop-cast from CB and CB, respectively.

The microscopic morphology of the pristine and doped films is further characterized by atomic force microscopy (AFM) (Figure 4). Both the pristine PODTT-4T<sub>CF</sub> and pristine PODTT-4T<sub>CB</sub> films are smooth with an average roughness of 1.2 nm and 5.0 nm, respectively. Pristine PODTT-4T<sub>CF</sub> shows a fibrous zone while PODTT-4T<sub>CB</sub> film looks amorphous, which is consistent with the GIWAXS results. The surface roughness of doped films is slightly increased, which is in agreement with the enlarged crystalline domains observed in GIWAXS. For the doped PODTT-4T<sub>CF</sub> film, the self-aggregation of dopants is not obviously observed at the surface compared to that of PODTT-4T<sub>CB</sub> film, suggesting better miscibility of FeCl<sub>3</sub> with the former film. The GIWAXS information and AFM results support the fact that the ordered molecular packing and higher crystallinity in PODTT-4T<sub>CF</sub> film are responsible for its higher mobility compared to that of PODTT-4T<sub>CB</sub> film. The use of chloroform solvent can promote polymer chains to form more ordered packing and larger crystalline domains.

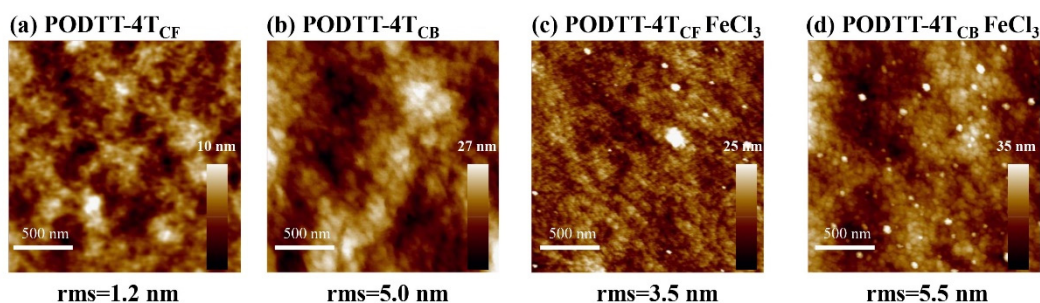


**Figure 4.** AFM height images of (a) pristine PODTT-4T<sub>CF</sub> film, (b) pristine PODTT-4T<sub>CB</sub> film, (c) doped PODTT-4T<sub>CF</sub> film, and (d) doped PODTT-4T<sub>CB</sub> film.

To further elucidate the carrier transport mechanism in the doped PODTT-4T<sub>CF</sub> and PODTT-4T<sub>CB</sub> films, the temperature-dependent  $\sigma$  was measured. It has been found that the  $\sigma$  increases with increased temperature (Figure 5), indicating thermal activated transport properties in doped films [34,35]. The transport activation energy ( $E_a$ ) of the doped PODTT-4T<sub>CF</sub> film and PODTT-4T<sub>CB</sub> film can be calculated according to the equation of  $\sigma = \sigma_0 \exp(-E_a/k_B T)$ , where  $\sigma_0$  is the pre-exponential conductivity and  $k_B$  is Boltzmann constant [35]. It has been found that the  $E_a$  of the doped PODTT-4T<sub>CF</sub> film is 5.2 meV, which is lower than that of doped PODTT-4T<sub>CB</sub> films ( $E_a = 8.0$  meV). The low  $E_a$  suggests a low transport barrier exists, and thus more polaronic states can contribute to electrical conductivity due to the continuous carrier transport channels in the doped PODTT-4T<sub>CF</sub> film [36]. Therefore, the film prepared from CF solution allows highly ordered and crystalline domains, resulting in strong coupling between doped polymer chains and thus a high carrier mobility.

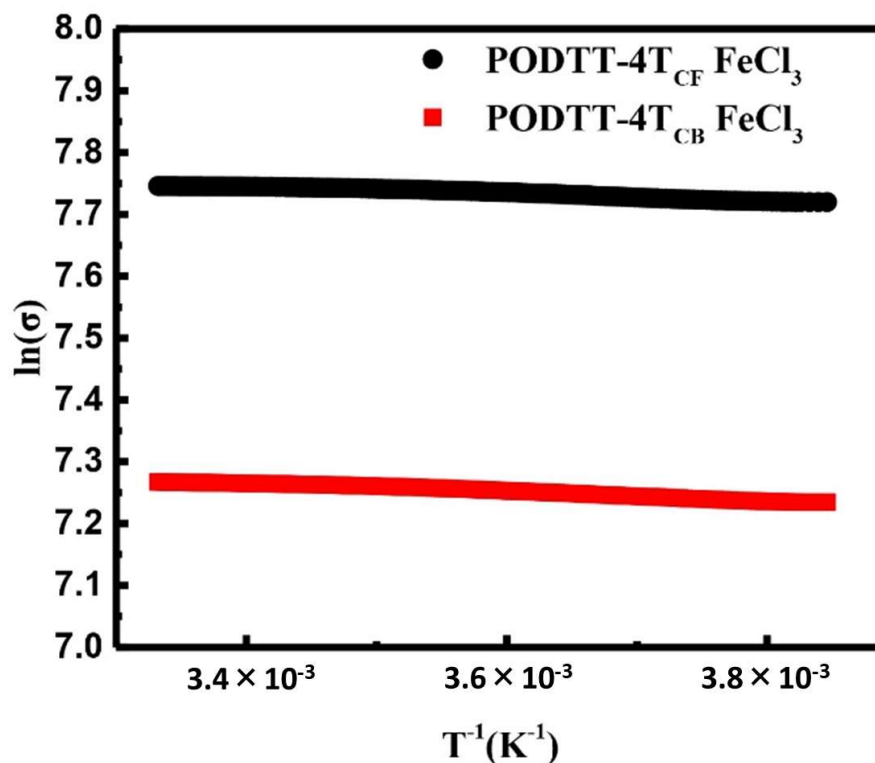


**Figure 5.** Temperature-dependent electrical conductivity of doped PODTT-4T<sub>CF</sub> and PODTT-4T<sub>CB</sub> films (the unit of  $\sigma$  is S cm<sup>-1</sup>). All doped films were immersed in FeCl<sub>3</sub> solution for 10 min.

#### 4. Conclusions

In this work, the effect of solvent on morphology, doping process and electrical conductivity of thiophene polymers has been investigated. It has been found that the molecular orientation in films is strongly related to the solvent used for dissolving the polymer, which is dominated by the evaporation rate of solvent during film formation. The films prepared from chloroform (PODTT-4T<sub>CF</sub>) mainly have an edge-on orientation, while the films prepared from chlorobenzene (PODTT-4T<sub>CB</sub>) show both edge-on and face-on orientations. PODTT-4T<sub>CF</sub> film exhibits better crystallinity than that of the chlorobenzene-processed film. The crystallinity has significant influence on charge transport properties rather than the doping level. As a result, FeCl<sub>3</sub>-doped PODTT-4T<sub>CF</sub> film shows a higher electrical conductivity of up to 408 S cm<sup>-1</sup> and is attributed to a high carrier mobility correlated to the continuous and largely crystalline domains in film compared to that of chlorobenzene-processed film. Our findings show that the selection of solvents for the preparation of film is a promising strategy to optimize the electrical conductivity of doped polymers.

**Supplementary Materials:** The following supporting information can be downloaded at: <https://www.mdpi.com/article/10.3390/ma15093293/s1>, Figure S1: GPC trace of PODTT-4T; Figure S2: TGA curve of PODTT-4T; Figure S3: DSC scan curves of PODTT-4T; Figure S4: Cyclic voltammetry profiles of PODTT-4T; Figure S5: Thermoelectric performance; Figure S6: Hall effect measurement; Figure S7: 2D-GIWAXS images; Table S1: The ratio of the integrated area between (bi)polaron band and the neutral band; Table S2: Raman spectroscopy; Table S3: The mobility and carrier concentration; Table S4: Data of 2D-GIWAXS.

**Author Contributions:** H.L. conceived the idea and designed the experiments; H.C. performed the experiments and analyzed the data; F.Z. and Z.X. discussed the results; H.C. and H.L. wrote the paper; S.B. and L.C. discussed the results and commented on the manuscript. All authors have read and agreed to the published version of the manuscript.

**Funding:** This research was funded by the National Natural Science Foundation of China (No. 21905294) and the Shanghai Sailing Program. The authors acknowledge beam-time provided by beamline BL14B1 (Shanghai Synchrotron Radiation Facility).

**Institutional Review Board Statement:** Not applicable.

**Informed Consent Statement:** Not applicable.

**Data Availability Statement:** The data that supports the findings of this study are available from the corresponding author upon reasonable request.

**Conflicts of Interest:** The authors declare no conflict of interest.

#### References

1. Heeger, A.J. Semiconducting and Metallic Polymers: The Fourth Generation of Polymeric Materials (Nobel Lecture). *Angew. Chem. Int. Ed.* **2001**, *40*, 2591–2611. [[CrossRef](#)]
2. Forrest, S.R. The path to ubiquitous and low-cost organic electronic appliances on plastic. *Nature* **2004**, *428*, 911–918. [[CrossRef](#)] [[PubMed](#)]
3. Russ, B.; Gludell, A.; Urban, J.J.; Chabiny, M.L.; Segalman, R.A. Organic thermoelectric materials for energy harvesting and temperature control. *Nat. Rev. Mater.* **2016**, *1*, 16050. [[CrossRef](#)]
4. Wang, Y.; Yang, L.; Shi, X.L.; Shi, X.; Chen, L.; Dargusch, M.S.; Zou, J.; Chen, Z.G. Flexible Thermoelectric Materials and Generators: Challenges and Innovations. *Adv. Mater.* **2019**, *31*, e1807916. [[CrossRef](#)]
5. Zhang, Q.; Sun, Y.; Xu, W.; Zhu, D. Organic thermoelectric materials: Emerging green energy materials converting heat to electricity directly and efficiently. *Adv. Mater.* **2014**, *26*, 6829–6851. [[CrossRef](#)]
6. He, J.; Tritt, T.M. Advances in thermoelectric materials research: Looking back and moving forward. *Science* **2017**, *357*, 1369. [[CrossRef](#)]
7. Yan, H.; Ma, W. Molecular Doping Efficiency in Organic Semiconductors: Fundamental Principle and Promotion Strategy. *Adv. Funct. Mater.* **2021**, *32*, 2111351. [[CrossRef](#)]
8. Zhao, W.; Ding, J.; Zou, Y.; Di, C.A.; Zhu, D. Chemical doping of organic semiconductors for thermoelectric applications. *Chem. Soc. Rev.* **2020**, *49*, 7210–7228. [[CrossRef](#)]

9. Yamashita, Y.; Tsurumi, J.; Ohno, M.; Fujimoto, R.; Kumagai, S.; Kurosawa, T.; Okamoto, T.; Takeya, J.; Watanabe, S. Efficient molecular doping of polymeric semiconductors driven by anion exchange. *Nature* **2019**, *572*, 634–638. [[CrossRef](#)]
10. Deng, L.; Chen, G. Recent progress in tuning polymer oriented microstructures for enhanced thermoelectric performance. *Nano Energy* **2021**, *80*, 105448. [[CrossRef](#)]
11. Patel, S.N.; Glaudell, A.M.; Peterson, K.A.; Thomas, E.M.; O'Hara, K.A.; Lim, E.; Chabiny, M.L. Morphology controls the thermoelectric power factor of a doped semiconducting polymer. *Sci. Adv.* **2017**, *3*, e1700434. [[CrossRef](#)] [[PubMed](#)]
12. Hynynen, J.; Kiefer, D.; Müller, C. Influence of crystallinity on the thermoelectric power factor of P3HT vapour-doped with F4TCNQ. *RSC Adv.* **2018**, *8*, 1593–1599. [[CrossRef](#)]
13. Wu, L.; Li, H.; Chai, H.; Xu, Q.; Chen, Y.; Chen, L. Anion-Dependent Molecular Doping and Charge Transport in Ferric Salt-Doped P3HT for Thermoelectric Application. *ACS Appl. Electron. Mater.* **2021**, *3*, 1252–1259. [[CrossRef](#)]
14. Zhang, Q.; Sun, Y.; Xu, W.; Zhu, D. What To Expect from Conducting Polymers on the Playground of Thermoelectricity: Lessons Learned from Four High-Mobility Polymeric Semiconductors. *Macromolecules* **2014**, *47*, 609–615. [[CrossRef](#)]
15. Jacobs, I.E.; Aasen, E.W.; Oliveira, J.L.; Fonseca, T.N.; Roehling, J.D.; Li, J.; Zhang, G.; Augustine, M.P.; Mascall, M.; Moulé, A.J. Comparison of solution-mixed and sequentially processed P3HT:F4TCNQ films: Effect of doping-induced aggregation on film morphology. *J. Mater. Chem. C* **2016**, *4*, 3454–3466. [[CrossRef](#)]
16. Scholes, D.T.; Yee, P.Y.; McKeown, G.R.; Li, S.; Kang, H.; Lindemuth, J.R.; Xia, X.; King, S.C.; Seferos, D.S.; Tolbert, S.H.; et al. Designing Conjugated Polymers for Molecular Doping: The Roles of Crystallinity, Swelling, and Conductivity in Sequentially-Doped Selenophene-Based Copolymers. *Chem. Mater.* **2018**, *31*, 73–82. [[CrossRef](#)]
17. Nam, G.-H.; Sun, C.; Chung, D.S.; Kim, Y.-H. Enhancing Doping Efficiency of Diketopyrrolopyrrole-Copolymers by Introducing Sparse Intramolecular Alkyl Chain Spacing. *Macromolecules* **2021**, *54*, 7870–7879. [[CrossRef](#)]
18. Liu, J.; Ye, G.; Potgieser, H.G.O.; Koopmans, M.; Sami, S.; Nugraha, M.I.; Villalva, D.R.; Sun, H.; Dong, J.; Yang, X.; et al. Amphiphathic Side Chain of a Conjugated Polymer Optimizes Dopant Location toward Efficient N-Type Organic Thermoelectrics. *Adv. Mater.* **2021**, *33*, e2006694. [[CrossRef](#)]
19. Li, H.; DeCoster, M.E.; Ming, C.; Wang, M.; Chen, Y.; Hopkins, P.E.; Chen, L.; Katz, H.E. Enhanced Molecular Doping for High Conductivity in Polymers with Volume Freed for Dopants. *Macromolecules* **2019**, *52*, 9804–9812. [[CrossRef](#)]
20. Kroon, R.; Kiefer, D.; Stegerer, D.; Yu, L.; Sommer, M.; Muller, C. Polar Side Chains Enhance Processability, Electrical Conductivity, and Thermal Stability of a Molecularly p-Doped Polythiophene. *Adv. Mater.* **2017**, *29*, 1700930. [[CrossRef](#)]
21. Kiefer, D.; Kroon, R.; Hofmann, A.I.; Sun, H.; Liu, X.; Giovannitti, A.; Stegerer, D.; Cano, A.; Hynynen, J.; Yu, L.; et al. Double doping of conjugated polymers with monomer molecular dopants. *Nat. Mater.* **2019**, *18*, 149–155. [[CrossRef](#)] [[PubMed](#)]
22. An, T.K.; Kang, I.; Yun, H.J.; Cha, H.; Hwang, J.; Park, S.; Kim, J.; Kim, Y.J.; Chung, D.S.; Kwon, S.K.; et al. Solvent Additive to Achieve Highly Ordered Nanostructural Semicrystalline DPP Copolymers: Toward a High Charge Carrier Mobility. *Adv. Mater.* **2013**, *25*, 7003–7009. [[CrossRef](#)] [[PubMed](#)]
23. Di, B.C.; Lu, K.; Zhang, L.; Liu, Y.; Guo, Y.; Sun, X.; Wen, Y.; Yu, G.; Zhu, D. Solvent-Assisted Re-annealing of Polymer Films for Solution-Processable Organic Field-Effect Transistors. *Adv. Mater.* **2010**, *22*, 1273–1277. [[CrossRef](#)] [[PubMed](#)]
24. Li, H.; Song, J.; Xiao, J.; Wu, L.; Katz, H.E.; Chen, L. Synergistically Improved Molecular Doping and Carrier Mobility by Copolymerization of Donor–Acceptor and Donor–Donor Building Blocks for Thermoelectric Application. *Adv. Funct. Mater.* **2020**, *30*, 2004378. [[CrossRef](#)]
25. Liu, Q.; Kumagai, S.; Manzhos, S.; Chen, Y.; Angunawela, I.; Nahid, M.M.; Feron, K.; Bottle, S.E.; Bell, J.; Ade, H.; et al. Synergistic Use of Pyridine and Selenophene in a Diketopyrrolopyrrole-Based Conjugated Polymer Enhances the Electron Mobility in Organic Transistors. *Adv. Funct. Mater.* **2020**, *30*, 2000489. [[CrossRef](#)]
26. Ding, J.; Liu, Z.; Zhao, W.; Jin, W.; Xiang, L.; Wang, Z.; Zeng, Y.; Zou, Y.; Zhang, F.; Yi, Y.; et al. Selenium-Substituted Diketopyrrolopyrrole Polymer for High-Performance p-Type Organic Thermoelectric Materials. *Angew. Chem. Int. Ed.* **2019**, *58*, 18994–18999. [[CrossRef](#)]
27. Müller, L.; Nanova, D.; Glaser, T.; Beck, S.; Pucci, A.; Kast, A.K.; Schröder, R.R.; Mankel, E.; Pingel, P.; Neher, D.; et al. Charge-Transfer–Solvent Interaction Predefines Doping Efficiency in p-Doped P3HT Films. *Chem. Mater.* **2016**, *28*, 4432–4439. [[CrossRef](#)]
28. Francis, C.; Fazzi, D.; Grimm, S.B.; Paulus, F.; Beck, S.; Hillebrandt, S.; Pucci, A.; Zaumseil, J. Raman spectroscopy and microscopy of electrochemically and chemically doped high-mobility semiconducting polymers. *J. Mater. Chem. C* **2017**, *5*, 6176–6184. [[CrossRef](#)]
29. Paternò, G.M.; Robbiano, V.; Fraser, K.J.; Frost, C.; García Sakai, V.; Cacialli, F. Neutron Radiation Tolerance of Two Benchmark Thiophene-Based Conjugated Polymers: The Importance of Crystallinity for Organic Avionics. *Sci. Rep.* **2017**, *7*, 41013. [[CrossRef](#)]
30. Li, Y.; Singh, S.P.; Sonar, P. A high mobility P-type DPP-thieno[3,2-b]thiophene copolymer for organic thin-film transistors. *Adv. Mater.* **2010**, *22*, 4862–4866. [[CrossRef](#)]
31. Li, H.; Xu, Z.; Song, J.; Chai, H.; Wu, L.; Chen, L. Single-Solution Doping Enabling Dominant Integer Charge Transfer for Synergistically Improved Carrier Concentration and Mobility in Donor–Acceptor Polymers. *Adv. Funct. Mater.* **2021**, *32*, 2110047. [[CrossRef](#)]
32. Rivnay, J.; Mannsfeld, S.C.; Miller, C.E.; Salleo, A.; Toney, M.F. Quantitative determination of organic semiconductor microstructure from the molecular to device scale. *Chem. Rev.* **2012**, *112*, 5488–5519. [[CrossRef](#)] [[PubMed](#)]



33. Salleo, A.; Kline, R.J.; DeLongchamp, D.M.; Chabinyc, M.L. Microstructural characterization and charge transport in thin films of conjugated polymers. *Adv. Mater.* **2010**, *22*, 3812–3838. [[CrossRef](#)] [[PubMed](#)]
34. Shen, Y.; Diest, K.; Wong, M.H.; Hsieh, B.R.; Dunlap, D.H.; Malliaras, G.G. Charge transport in doped organic semiconductors. *Phys. Rev. B* **2003**, *68*, 081204. [[CrossRef](#)]
35. Un, H.; Gregory, S.A.; Mohapatra, S.K.; Xiong, M.; Longhi, E.; Lu, Y.; Rigin, S.; Jhulki, S.; Yang, C.; Timofeeva, T.V.; et al. Understanding the Effects of Molecular Dopant on n-Type Organic Thermoelectric Properties. *Adv. Energy Mater.* **2019**, *9*, 1900817. [[CrossRef](#)]
36. Gregory, S.A.; Menon, A.K.; Ye, S.; Seferos, D.S.; Reynolds, J.R.; Yee, S.K. Effect of Heteroatom and Doping on the Thermoelectric Properties of Poly(3-alkylchalcogenophenes). *Adv. Energy Mater.* **2018**, *8*, 1802419. [[CrossRef](#)]